IEEE Access
Multidisciplinary | Rapid Review | Open Access Journal

Received January 9, 2021, accepted January 17, 2021, date of publication January 25, 2021, date of current version February 2, 2021.

Digital Object Identifier 10.1109/ACCESS.2021.3054007

High-Accurate Non-Uniform Grids for System-Combined ADI-FDTD Method in Near-Field Scattering With Proper CFL Factor

NAIXING FENG[1], (Member, IEEE), YUXIAN ZHANG[1], (Member, IEEE), JINFENG ZHU[2,3], (Senior Member, IEEE), QINGSHENG ZENG[4], (Senior Member, IEEE), AND GUO PING WANG[1]

[1]Institute of Microscale Optoelectronics, Shenzhen University, Shenzhen 518060, China
[2]Institute of Electromagnetics and Acoustics, Xiamen University, Xiamen 361005, China
[3]Department of Electronic Science, Xiamen University, Xiamen 361005, China
[4]College of Astronautics, Nanjing University of Aeronautics and Astronautics, Nanjing 210016, China

Corresponding author: Yuxian Zhang (yxzhang_tute@126.com)

This work was supported in part by the National Natural Science Foundation of China under Grant 61901274 and Grant 11734012, in part by the Natural Science Foundation of Guangdong Province under Grant 2020A1515010467, and in part by the Shenzhen Science and Technology Innovation Committee under Grant JCYJ20190808141818890.

ABSTRACT In this paper, a high-accurate technique with non-uniform grids is introduced into a system-combined alternative-direction-implicit finite-difference time-domain (SC-ADI-FDTD) algorithm, and then successfully used to analyze electromagnetic propagations. To our knowledge, the conventional FDTD with non-uniform grids can be effectively deal with some edges of the three-dimensional cubes and complicated structures of the tiny objects by modulating the local grid scales, which to the extent improves its reliability and accuracy. However, due to existing the finer grids in the local computational region and the inevitable Courant-Friedrichs-Lewy (CFL) limit in the conventional FDTD, the temporal interval must be determined by the minimum fine spatial grid, resulting in much larger temporal sampling density required during the whole computation process. As the advantage of circumventing the repeated variables, the non-uniform SC-ADI-FDTD (NUSC-ADI-FDTD) cannot only break through the CFL limit to implement the high-efficient computation, but also further save more CPU time in the local microstructure cases. Furthermore, the empirical formula between the spatial sampling density and the CFL factors can be obtained from the numerical fitting method after errors analysis. The numerical simulations of the electromagnetic scattering have been executed to illustrate feasibility and validity of our proposed method.

INDEX TERMS Courant-Friedrichs-Lewy (CFL) limit, electromagnetic propagations, local microstructure problems, non-uniform SC-ADI-FDTD (NUSC-ADI-FDTD).

I. INTRODUCTION

Nowadays, many numerical methods in the modern electromagnetic theory have been developed by human wisdom to gradually replace experimental measurements with numerical simulations so that some unnecessary costs from the expensive devices and equipments can be substantially circumvented during the repetitive experiment. However, under the circumstance of keeping the enough satisfactory numerical accuracy, we must mainly concentrate on how to improve the computational efficiency to the extent, which has become the focus and difficult point of electromagnetic numerical methods.

Generally speaking, the FDTD method [1], [2] can be effective in solving electromagnetic problems in recent years, for example, the near-field acquisition [3], and the research of Bloch-Floquet periodic boundary [4] *et al*. On the other hand, the non-uniform technique [5], [6] is effectively developed

The associate editor coordinating the review of this manuscript and approving it for publication was Muhammad Zubair.

to decrease the inevitable numerical errors from the three-dimensional (3D) modeling during the conventional FDTD method, therefore, the higher numerical accuracy can be obtained for the grid initialization by applying the non-uniform FDTD (NU-FDTD) method. In 1996, Navarro *et al.* [7] firstly made use of the NU-FDTD method for analyzing waveguide structure and perfectly matched layer (PML). Afterward, Shen *et al.* [8] utilized the NU-FDTD method for the efficient analysis of propagation characteristics of optical-fiber waveguides in the cylindrical coordinate system. Meanwhile, Yu and Mittra [9], [10] came up with an optimal method of the NU-FDTD method to process the coaxial discontinuity structure. Li *et al*. [11] also designed a microstrip structure with the effective PML truncation via the 3D NU-FDTD. In 2002, Zhang *et al.* [12] successfully analyzed and studied quasi-network characteristics through the NU-FDTD method. In 2010, both Li and Hu [13] employed the NU-FDTD to observe and study the magneto-plasma antenna. In 2015, compared with the conventional FDTD under the fine and coarse grids, Elsherbeni and Demir [14] adopt 3D non-uniform grids to work for the patch antenna and low-pass filter. In fact, the unstructured meshes are discussed in other numerical methods such as discontinuous Galerkin time-domain method [15], which have the higher advantage in object subdivision. However, the non-uniform grids show more convenience in geometry modeling.

To the best of our knowledge, the iteration in the conventional FDTD is constrained by the Courant-Friedrichs-Lewy (CFL) condition. Although the non-uniform technique is adopted to increase grid densities for the local regions so that the numerical accuracy can be enhanced, the computational efficiencies for a fine-grid region in the NU-FDTD method are not dramatically improved due to the upper CFL limit and the smaller time interval leads to obvious deterioration. Consequently, in order to further raise efficiency, we are quite necessary to develop a corresponding and reliable method for conquering the CFL limit with the larger time interval, when encountering more complicated research problems.

Fortunately, to overcome the CFL limit, Namiki [16] proposed the alternating-direction-implicit (ADI) scheme applied into the FDTD method firstly in 1999. About the same time, Zheng *et al.* [17], [18] further developed the ADI-FDTD method for the 3D electromagnetic simulations. Lee and Fornberg [19] adopted the extremely high spatial density to show the error curves for some unconditionally stable time stepping methods. To effectively solve the 3D cavity resonance problem, Sun and Choi [20] introduced the non-uniform technique into the ADI-FDTD method. The leapfrog ADI-FDTD [21] in 3D cases are proposed in the different research fields such as dispersive media [22] and domain decomposition [23]. The unconditionally stable algorithm also involves Crank-Nicolson FDTD [24], locally one-dimensional FDTD [25], Multiple 1-D ADI-FDTD [26], [27], and so on. In recent years, several new developments step into the ADI-FDTD method. In 2019, Zheng *et al*. [28] proposed the conformal ADI-FDTD method applied for tackling with the wide-band modeling on-chip spiral inductors, and Chen *et al.* [29] presented the ADI-FDTD algorithm for simulating graphene-based frequency-selective surface in the terahertz frequency. At the same time, Feng *et al.* [30] developed the system-combined ADI-FDTD (SC-ADI-FDTD) applied to microwave technique and antenna design, which can avoid the repeated computation of the conventional ADI-FDTD method by the signal chart. In this paper, we are going to introduce the non-uniform grids into the SC-ADI-FDTD used for analyzing the local micro-structure scattering. The main contributions of this work are:

(*a*) The non-uniform SC-ADI-FDTD (NUSC-ADI-FDTD) is used to overcome the CFL limit, and obtain the similar computational efficiency when CFL factor equals to about 1.50 as the conventional NU-FDTD method;

(*b*) Under the circumstance of keeping the satisfactory accuracy, the proper CFL factor can be given by the empirical formula and the proposed NUSC-ADI-FDTD method can be used to effectively solve the 3D electromagnetic propagation of the local micro-structure objects.

The organization of this paper is as follow. In section II, we introduce the initialization and formula of non-uniform grids between the fine grids and coarse grids. The iteration of the NUSC-ADI-FDTD method is shown in section III. In section IV, compared with the conventional NU-FDTD method, we solve three numerical simulations of the 3D electromagnetic scattering by the NUSC-ADI-FDTD, and record those CPU time to verify our proposed method. Finally, we will draw the conclusion in section V.

II. INITIALIZATION AND FORMULA OF NON-UNIFORM GRIDS

How to initialize the grid scale in the conventional FDTD method is an important and necessary balance between the computational time and the specific numerical accuracy. It is well known that the homogeneous meshing by utilizing the fine grids can be adopted to construct the geometry more accurately. When facing the spatial meshing in the 3D cases, the computational time will be increased by 16 times, if the grid scale is reduced to the half. Unfortunately, for the local micro-structure electromagnetic problem, on the one hand, a higher-density meshing cannot be avoided in the tiny geometry or the small two-object's distance. On the other hand, a large number of grids are inevitably occurred for the larger single-material region or the longer distance between some objects so that the computer memory will be always wasted. Therefore, under the situation of enhancing the computational efficiency and reducing the computer memory, the non-uniform grids are an excellent way to solve a local small-scale problem due to the fact that the different grid units in size can be applied in the different regions. As shown in Fig. 1, the non-uniform grids are the key to build the bridge between coarse and fine grids corresponding to large and small region.

In the first time, the coarse grids are the initialization as a background cell for the NU-FDTD method, whereas the fine

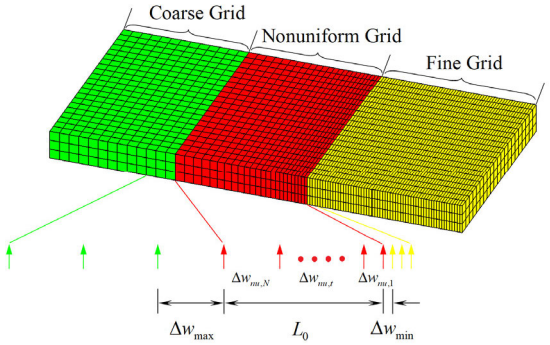

FIGURE 1. The diagram of non-uniform grids between the coarse and fine grids.

grids are only necessary to build for the microscale region. In fact, to avoid the numerical mutation from the geometry modeling, we employ the gradually smoothing processing to implement the non-uniform grids between coarse and fine grids. The scale $\Delta w_{\max}$ and $\Delta w_{\min}$ represents respectively the grids interval for the coarse and fine region. In non-uniform grids, the interval between every node can be directly defined below

$$\Delta w_{nu,t} = L^t \Delta w_{\min} \tag{1}$$

where t is the number in the non-uniform grid area and L is the base number for the exponential change. $\Delta w_{\min}$ and $\Delta w_{\max}$ are respectively denoted as the size of the fine grid when $t = 0$ and the coarse grid when $t = N + 1$, and $\Delta w_{nu,t}$ represents the different-grid size for $t = 1, 2, \ldots, N$. Hence, the whole length L_0 in the non-uniform grid region satisfies below

$$L_0 = \sum_{t=1}^{N} L^t \Delta w_{\min} \tag{2}$$

Applying the geometric progression, we can obtain

$$\Delta w_{\min} + L_0 + \Delta w_{\max} = \frac{\Delta w_{\min} - L\Delta w_{\max}}{1 - L} \tag{3}$$

From the equation (3), the base number L is the same to achieve the exponential change, expressed as

$$L = \frac{L_0 + \Delta w_{\max}}{L_0 + \Delta w_{\min}} \tag{4}$$

Incorporate the equation (4) into the equation (2), the whole grid number N can be determined in the non-uniform region

$$N = \frac{\ln \Delta w_{\max} - \ln \Delta w_{\min}}{\ln L_0} - 1 \tag{5}$$

According to the above node distribution, we can build the corresponding discretization for all the geometries in the 3D Cartesian coordinate can be confirmed.

III. ITERATIVE FORMULAS OF NUSC-ADI-FDTD METHOD

Referring to [30], we have understood the high efficiency of the SC-ADI-FDTD method and further summarize those iterative formulas with the intermediate vectors $\boldsymbol{T}_{H1}$ and $\boldsymbol{T}_{H2}$ which can avoid the repeated computation for the conventional ADI-FDTD. The two procedure of the SC-ADI-FDTD method can be given as follow

First procedure:

$$\boldsymbol{T}_{H1}^{n-\frac{1}{4}} = \mathbf{C}_{HH}\boldsymbol{H}^{n-\frac{1}{4}} + \boldsymbol{T}_{H2}^{n-\frac{1}{4}} \tag{6}$$

$$\boldsymbol{\Phi}_1\boldsymbol{E}^{n+\frac{1}{2}} = \mathbf{C}_{EE}\boldsymbol{E}^{n} + \boldsymbol{T}_{H1}^{n-\frac{1}{4}} - \mathbf{C}_{EHB}\boldsymbol{H}^{n-\frac{1}{4}} \tag{7}$$

$$\boldsymbol{T}_{H2}^{n+\frac{1}{4}} = \mathbf{C}_{HEB}\boldsymbol{E}^{n+\frac{1}{2}} \tag{8}$$

$$\boldsymbol{H}^{n+\frac{1}{4}} = \boldsymbol{T}_{H1}^{n-\frac{1}{4}} + \boldsymbol{T}_{H2}^{n+\frac{1}{4}} \tag{9}$$

Second procedure:

$$\boldsymbol{T}_{H1}^{n+\frac{1}{4}} = \mathbf{C}_{HH}\boldsymbol{H}^{n+\frac{1}{4}} + \boldsymbol{T}_{H2}^{n+\frac{1}{4}} \tag{10}$$

$$\boldsymbol{\Phi}_2\boldsymbol{E}^{n+1} = \boldsymbol{C}_{EE}\boldsymbol{E}^{n+\frac{1}{2}} + \mathbf{C}_{EHA}\boldsymbol{H}^{n+\frac{1}{4}} - \mathbf{C}_{EHB}\boldsymbol{T}_{H1}^{n+\frac{1}{4}} \tag{11}$$

$$\boldsymbol{T}_{H2}^{n+\frac{3}{4}} = -\mathbf{C}_{HEA}\boldsymbol{E}^{n+1} \tag{12}$$

$$\boldsymbol{H}^{n+\frac{3}{4}} = \boldsymbol{T}_{H1}^{n+\frac{1}{4}} + \boldsymbol{T}_{H2}^{n+\frac{3}{4}} \tag{13}$$

where the vectors $\boldsymbol{E}$ and $\boldsymbol{H}$ are respectively the electric and magnetic fields. The matrices $\boldsymbol{\Phi}_1 = \mathbf{I} - \mathbf{C}_{EHA}\mathbf{C}_{HEB}$ and $\boldsymbol{\Phi}_2 = \mathbf{I} - \mathbf{C}_{EHB}\mathbf{C}_{HEA}$ are the unconditionally stable terms for implementing the iteration of electric fields. The symbols $\boldsymbol{T}_{H1}$ and $\boldsymbol{T}_{H2}$ are the prestore vectors for the SC-ADI-FDTD method. The general matrices from the conventional FDTD modeling can be easily defined below

$$\mathbf{C}_{HH} = \mathbf{C}_{HE}(\boldsymbol{\mu}\Delta t^{-1} - 0.5\boldsymbol{\sigma}_m) \tag{14}$$

$$\mathbf{C}_{HEA} = \mathbf{C}_{HE}\mathbf{A} \tag{15}$$

$$\mathbf{C}_{HEB} = \mathbf{C}_{HE}\mathbf{B} \tag{16}$$

$$\mathbf{C}_{EE} = \mathbf{C}_{EH}(\boldsymbol{\varepsilon}\Delta t^{-1} - 0.5\boldsymbol{\sigma}_e) \tag{17}$$

$$\mathbf{C}_{EHA} = \mathbf{C}_{EH}\mathbf{A} \tag{18}$$

$$\mathbf{C}_{EHB} = \mathbf{C}_{EH}\mathbf{B} \tag{19}$$

where both the matrices $\mathbf{C}_{HE}$ and $\mathbf{C}_{EH}$ are respectively

$$\mathbf{C}_{HE} = (\boldsymbol{\mu}\Delta t^{-1} + 0.5\boldsymbol{\sigma}_m)^{-1}$$
$$\mathbf{C}_{EH} = (\boldsymbol{\varepsilon}\Delta t^{-1} + 0.5\boldsymbol{\sigma}_e)^{-1}$$

and the differential matrices $\mathbf{A}$ and $\mathbf{B}$ are separated from the curl operation, shown as

$$\mathbf{A} = \begin{bmatrix} 0 & 0 & \partial_y \\ \partial_z & 0 & 0 \\ 0 & \partial_x & 0 \end{bmatrix}, \quad \mathbf{B} = \begin{bmatrix} 0 & \partial_z & 0 \\ 0 & 0 & \partial_x \\ \partial_y & 0 & 0 \end{bmatrix}.$$

It can be found that $\boldsymbol{\Phi}_1$ and $\boldsymbol{\Phi}_2$ present the tri-diagonal matrices in the electromagnetic problem with the whole isotropic media, which can be solved by the chasing method to obtain the vectors $\boldsymbol{E}^{n+\frac{1}{2}}$ and $\boldsymbol{E}^{n+1}$. Next, with the non-uniform grids $[\Delta x(i), \Delta y(j), \Delta z(k)]$ in the 3D case, the pseudo

codes of the NUSC-ADI-FDTD method in n^{th} timestep can be expressed in the y direction as follow:

First procedure:

$$T_{H1,y}\big|_{i+\frac{1}{2},j,k+\frac{1}{2}}^{n-\frac{1}{4}} = C_{HH}\big|_{i+\frac{1}{2},j,k+\frac{1}{2}} H_y\big|_{i+\frac{1}{2},j,k+\frac{1}{2}}^{n-\frac{1}{4}} + T_{H2,y}\big|_{i+\frac{1}{2},j,k+\frac{1}{2}}^{n-\frac{1}{4}} \tag{20}$$

$$\begin{aligned} d_{1y}\big|_{i,j+\frac{1}{2},k}^{n+\frac{1}{2}} &= C_{EE}\big|_{i,j+\frac{1}{2},k} E_y\big|_{i,j+\frac{1}{2},k}^{n} \\ &+ C_{EH}\big|_{i,j+\frac{1}{2},k} \frac{T_{H1,x}\big|_{i,j+\frac{1}{2},k+\frac{1}{2}}^{n-\frac{1}{4}} - T_{H1,x}\big|_{i,j+\frac{1}{2},k-\frac{1}{2}}^{n-\frac{1}{4}}}{\Delta z(k)} \\ &- C_{EH}\big|_{i,j+\frac{1}{2},k} \frac{H_z\big|_{i+\frac{1}{2},j+\frac{1}{2},k}^{n-\frac{1}{4}} - H_z\big|_{i-\frac{1}{2},j+\frac{1}{2},k}^{n-\frac{1}{4}}}{\Delta x(i)} \end{aligned} \tag{21}$$

$$a_{1y}\big|_{i,j+\frac{1}{2},k} E_y\big|_{i,j+\frac{1}{2},k+1}^{n+\frac{1}{2}} + b_{1y}\big|_{i,j+\frac{1}{2},k} E_y\big|_{i,j+\frac{1}{2},k}^{n+\frac{1}{2}} + c_{1y}\big|_{i,j+\frac{1}{2},k} E_y\big|_{i,j+\frac{1}{2},k-1}^{n+\frac{1}{2}} = d_{1y}\big|_{i,j+\frac{1}{2},k}^{n+\frac{1}{2}} \tag{22}$$

$$T_{H2,y}\big|_{i+\frac{1}{2},j,k+\frac{1}{2}}^{n+\frac{1}{4}} = C_{HE}\big|_{i+\frac{1}{2},j,k+\frac{1}{2}} \frac{E_z\big|_{i+1,j,k+\frac{1}{2}}^{n+\frac{1}{2}} - E_z\big|_{i,j,k+\frac{1}{2}}^{n+\frac{1}{2}}}{\Delta x(i)} \tag{23}$$

$$H_y\big|_{i+\frac{1}{2},j,k+\frac{1}{2}}^{n+\frac{1}{4}} = T_{H1,y}\big|_{i+\frac{1}{2},j,k+\frac{1}{2}}^{n-\frac{1}{4}} + T_{H2,y}\big|_{i+\frac{1}{2},j,k+\frac{1}{2}}^{n+\frac{1}{4}} \tag{24}$$

where the iterative coefficients in the left-hand side from the equation (22) are shown as

$$\begin{aligned} a_{1y}\big|_{i,j+\frac{1}{2},k} &= \frac{C_{EH}\big|_{i,j+\frac{1}{2},k}\, C_{HH}\big|_{i+\frac{1}{2},j,k+\frac{1}{2}}}{[\Delta z(k)]^2} \\ b_{1y}\big|_{i,j+\frac{1}{2},k} &= 1 - \frac{C_{EH}\big|_{i,j+\frac{1}{2},k}\,(C_{HH}\big|_{i,j+\frac{1}{2},k+\frac{1}{2}} + C_{HH}\big|_{i,j+\frac{1}{2},k-\frac{1}{2}})}{[\Delta z(k)]^2} \\ c_{1y}\big|_{i,j+\frac{1}{2},k} &= \frac{C_{EH}\big|_{i,j+\frac{1}{2},k}\, C_{HH}\big|_{i,j+\frac{1}{2},k-\frac{1}{2}}}{[\Delta z(k)]^2} \end{aligned}$$

Second procedure:

$$T_{H1,y}\big|_{i+\frac{1}{2},j,k+\frac{1}{2}}^{n+\frac{1}{4}} = C_{HH}\big|_{i+\frac{1}{2},j,k+\frac{1}{2}} H_y\big|_{i+\frac{1}{2},j,k+\frac{1}{2}}^{n+\frac{1}{4}} + T_{H2,y}\big|_{i+\frac{1}{2},j,k+\frac{1}{2}}^{n+\frac{1}{4}} \tag{25}$$

$$\begin{aligned} d_{2y}\big|_{i,j+\frac{1}{2},k}^{n+1} &= C_{EE}\big|_{i,j+\frac{1}{2},k} E_y\big|_{i,j+\frac{1}{2},k}^{n+\frac{1}{2}} \\ &+ C_{EH}\big|_{i,j+\frac{1}{2},k} \frac{H_x\big|_{i,j+\frac{1}{2},k+\frac{1}{2}}^{n+\frac{1}{4}} - H_x\big|_{i,j+\frac{1}{2},k-\frac{1}{2}}^{n+\frac{1}{4}}}{\Delta z(k)} \\ &- C_{EH}\big|_{i,j+\frac{1}{2},k} \frac{T_{H1,z}\big|_{i+\frac{1}{2},j+\frac{1}{2},k}^{n+\frac{1}{4}} - T_{H1,z}\big|_{i-\frac{1}{2},j+\frac{1}{2},k}^{n+\frac{1}{4}}}{\Delta x(i)} \end{aligned} \tag{26}$$

$$a_{2y}\big|_{i,j+\frac{1}{2},k} E_y\big|_{i+1,j+\frac{1}{2},k}^{n+1} + b_{2y}\big|_{i,j+\frac{1}{2},k} E_y\big|_{i,j+\frac{1}{2},k}^{n+1} + c_{2y}\big|_{i,j+\frac{1}{2},k} E_y\big|_{i-1,j+\frac{1}{2},k}^{n+1} = d_{2y}\big|_{i,j+\frac{1}{2},k}^{n+1} \tag{27}$$

$$T_{H2,y}\big|_{i+\frac{1}{2},j,k+\frac{1}{2}}^{n+\frac{3}{4}} = -C_{HE}\big|_{i+\frac{1}{2},j,k+\frac{1}{2}} \frac{E_x\big|_{i+\frac{1}{2},j,k+1}^{n+1} - E_x\big|_{i+\frac{1}{2},j,k}^{n+1}}{\Delta z(k)} \tag{28}$$

$$H_y\big|_{i+\frac{1}{2},j,k+\frac{1}{2}}^{n+\frac{3}{4}} = T_{H1,y}\big|_{i+\frac{1}{2},j,k+\frac{1}{2}}^{n+\frac{1}{4}} + T_{H2,y}\big|_{i+\frac{1}{2},j,k+\frac{1}{2}}^{n+\frac{3}{4}} \tag{29}$$

where the iterative coefficients in the left-hand side from the equation (27) are expressed as

$$\begin{aligned} a_{2y}\big|_{i,j+\frac{1}{2},k} &= \frac{C_{EH}\big|_{i,j+\frac{1}{2},k}\, C_{HH}\big|_{i+\frac{1}{2},j+\frac{1}{2},k}}{[\Delta x(i)]^2} \\ b_{2y}\big|_{i,j+\frac{1}{2},k} &= 1 - \frac{C_{EH}\big|_{i,j+\frac{1}{2},k}\,(C_{HH}\big|_{i+\frac{1}{2},j+\frac{1}{2},k} + C_{HH}\big|_{i-\frac{1}{2},j+\frac{1}{2},k})}{[\Delta x(i)]^2} \\ c_{2y}\big|_{i,j+\frac{1}{2},k} &= \frac{C_{EH}\big|_{i,j+\frac{1}{2},k}\, C_{HH}\big|_{i-\frac{1}{2},j+\frac{1}{2},k}}{[\Delta x(i)]^2} \end{aligned}$$

In the similar way, we can obtain the other fields iteration of the NUSC-ADI-FDTD method in x and z direction according to those pseudo code. Therefore, in order to satisfy the numerical accuracy of the NUSC-ADI-FDTD method, we will introduce how to choose a proper CFL factor in the next section.

IV. PROPER CFL FACTOR WITH EMPIRICAL FORMULA

It is well known that the numerical accuracy of FDTD method is closely related with the temporal and spatial intervals. When fixing the maximum frequency $f_{\max}$ in our required region, the temporal and spatial sampling density can be defined based on those intervals $[\Delta x(i), \Delta y(j), \Delta z(k), \Delta t]$ from the FDTD initialization. The spatial sampling density Q_s refers to the number of points per wavelength (PPW), while the temporal sampling density Q_t represents the number of points per period (PPP).

$$Q_{s,w}(\text{PPW}) = \frac{\lambda_{\min}}{\Delta w_{\max}} = \frac{c_0}{f_{\max}\Delta w_{\max}\sqrt{\varepsilon_{r,\max}\mu_{r,\max}}} \tag{30}$$

$$Q_t(\text{PPP}) = \frac{T_{\min}}{\Delta t} = \frac{1}{f_{\max}\Delta t} \tag{31}$$

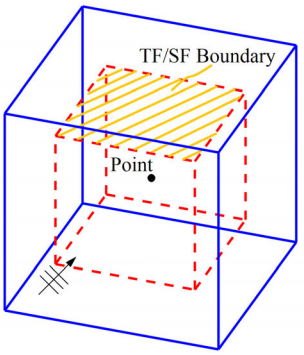

FIGURE 2. The obliquely plane-wave incidence for the TF/SF boundary in 3D case.

TABLE 1. The distribution of temporal sampling density (PPP) in the different spatial sampling density (PPW).

Spatial Sampling Density (PPW)	CFL Factor s					
	1	2	4	8	16	32
1200	2079.0	1038.5	519.3	259.6	129.8	64.9
600	1038.5	519.3	259.6	129.8	64.9	32.5
300	519.3	259.6	129.8	64.9	32.5	16.2
150	259.6	129.8	64.9	32.5	16.2	8.11
75	129.8	64.9	32.5	16.2	8.11	4.05

where the variables $\lambda_{\min}$, $T_{\min}$ and c_0 are respective the minimum wavelength, the minimum period and the light velocity in the air, and $\Delta w_{\max}$ is the maximum scale for the spatial intervals $[\Delta x(i), \Delta y(j), \Delta z(k)]$. With the specific media, those parameters about the maximum relative permittivity $\varepsilon_{r,\max}$, the maximum relative permeability $\mu_{r,\max}$ and the light velocity $v_{0,\min}$ need to be involved in the FDTD initialization. Both the equations (30) and (31) are dominated by the time-domain impulse from its maximum $f_{\max}$.

In the NUSC-ADI-FDTD method, with the CFL factor s, the temporal interval must satisfy

$$\Delta t = \frac{s}{\sqrt{3}c_0}\Delta w_{\min} \tag{32}$$

where $\Delta w_{\min}$ is defined as the minimum grid scale in the non-uniform grids. To obtain the empirical formula about the proper CFL factor s, we assume the same values $\Delta w = \Delta w_{\min} = \Delta w_{\max}$ in the original SC-ADI-FDTD without the non-uniform grids. Then we simplify the model only in the air with the oblique plane-wave incidences as shown in Fig.2. Referring to [2] and [3], the blue-line region covers the whole simulation area, and the six faces of the red-line areas are the total-field/scattering-field (TF/SF) boundary. The obliquely plane-wave incidence propagates into TF/SF boundary from its corner and we can intercept the time-domain results at the observation point.

We adopt the 3D conventional FDTD method in CFL factor $s = 1$ as the reference results and execute the SC-ADI-FDTD method with these different CFL factor $s = 1$, 2, 4, 8, 16 and 32. As shown in the TABLE.1, those corresponding temporal

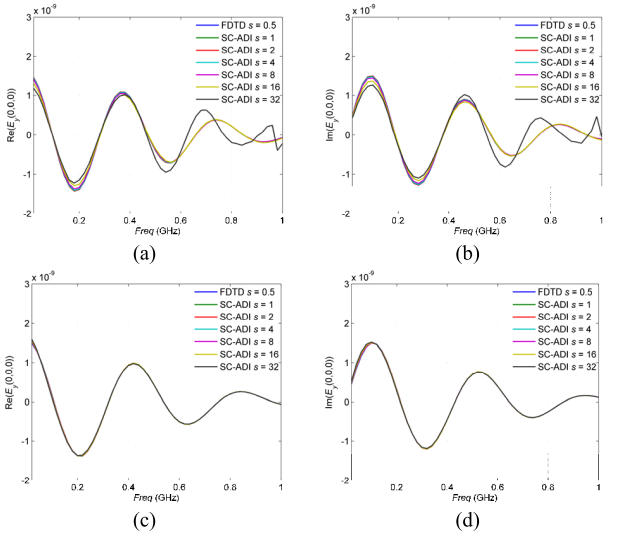

FIGURE 3. The electric fields E_y (0, 0, 0) in the frequency domain with the different CFL factors: (a) the real number of E_y (0, 0, 0) in 75 PPW; (b) the imaginary number of E_y (0, 0, 0) in 75 PPW; (c) the real number of E_y (0, 0, 0) in 1200 PPW; (d) the imaginary number of E_y (0, 0, 0) in 1200 PPW.

sampling density Q_t (PPP) can obtained. It can found that the temporal sampling density become smaller when the CFL factor s changes into the large number so that the general 3D unconditionally FDTD methods have the inevitably large errors after the computation. Therefore, we need to repeatedly carry out those processes and apply the relative norm error E_{rr} in the frequency domain after the time-domain results shown below

$$E_{rr} = \frac{\|\boldsymbol{x} - \boldsymbol{x}_{ref}\|}{\|\boldsymbol{x}_{ref}\|} \tag{33}$$

where the vector $\boldsymbol{x}$ denotes the numerical set of those SC-ADI-FDTD results and the vector $\boldsymbol{x}_{ref}$ represents the reference set from the conventional FDTD.

Over the time marching, the waveform of the input electric field is a Gaussian impulse with the incident angle $\theta_{inc} = 30°$ and $\varphi_{inc} = 60°$. The electric y-component E_y in the Cartesian coordinate (0, 0, 0) can be recorded in every timestep and transformed into the frequency domain. As shown in Fig.3 (a)-(b), with the increasing of the CFL factors, those numerical errors will be easily occurred when the spatial sampling density is very small.

However, depicted in the Fig.3 (c)-(d), the numerical accuracy still can be improved once enough spatial sampling density is given. Fortunately, compared with the conventional FDTD method, we can obtain the relative norm errors from the TABLE.2. Those errors executed from the 3D SC-ADI-FDTD method also can be drawn in Fig.4. As shown in TABLE.2 and Fig.4, under the different CFL factors, the norm errors keep the 2nd convergence with the increasing of the spatial sampling densities Q_s (PPW).

In order to ensure that those corresponding relative norm errors are controlled within about 1% from the TABLE 2, we can set the empirical formula between the spatial sampling

TABLE 2. The SC-ADI-FDTD norm errors with different CFL factor s in the different spatial sampling density Q_S (PPW).

Q_S (PPW)	CFL Factor s					
	1	2	4	8	16	32
1200	4.0×10^{-5}	1.1×10^{-4}	5.9×10^{-4}	0.0025	**0.0083**	0.0278
600	1.1×10^{-4}	3.8×10^{-4}	0.0013	0.0049	0.0142	0.0425
300	2.6×10^{-4}	0.0011	0.0036	**0.0112**	0.0341	0.0917
150	5.1×10^{-4}	0.0020	0.0073	0.0233	0.0658	0.1328
75	8.7×10^{-4}	0.0031	**0.0108**	0.0339	0.0856	0.1867

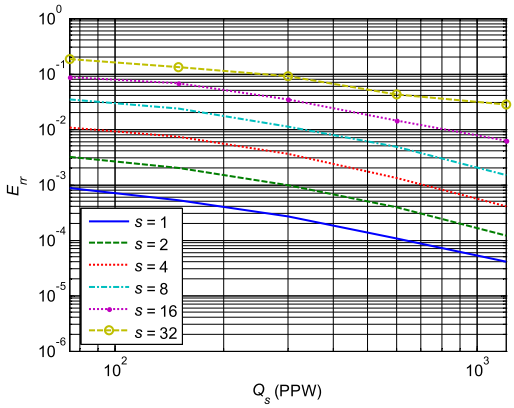

FIGURE 4. The norm error curves of amplitude E_y (0, 0, 0) from the SC-ADI-FDTD method in the frequency domain compared with the conventional FDTD method in $s = 0.5$. The different spatial sampling densities (PPW) are applied as the horizontal ordinate.

densities Q_s (PPW) and the CFL factor s expressed below

$$s = A_0 Q_s^{B_0} \tag{34}$$

After applying numerical fitting method by MATLAB curve toolbox, the parameter set (A_0, B_0) is (0.4619, 0.5) corresponding to the 1% norm errors, respectively. Therefore, with these processes, we forecast the proper CFL factors in the SC-ADI-FDTD method for the fine or non-uniform grids in maximum spatial sampling densities. To verify this empirical formula (34), we set the spatial sampling density $Q_s = 2400$ PPW and then can acquire the larger CFL factor $s = 22.62$. After the SC-ADI-FDTD computation, the norm error in this case is 0.0095 which satisfy the (34).

V. NUMERICAL EXPERIMENTS

A. SINGLE CUBE

To validate our proposed NUSC-ADI-FDTD method, we employ the TF/SF boundary condition to add the obliquely plane-wave incidence with the incident angle $\theta_{inc} = 45°$ and $\varphi_{inc} = 30°$ and compute the electromagnetic scattering for the single cube (160 mm × 160 mm × 160 mm) with dielectric medium parameter $\varepsilon_r = 16$ and $\mu_r = 1$. The single cube is surrounded with the air box (360 mm × 360 mm × 360 mm) as shown in the Fig.5(a).

The technique of the non-uniform grids are adopted which are displayed in Fig.5(b) and we can keeps the same spatial sampling density $Q_s = 30$ PPW between the coarse grids in air and the fine grids in the dielectric medium.

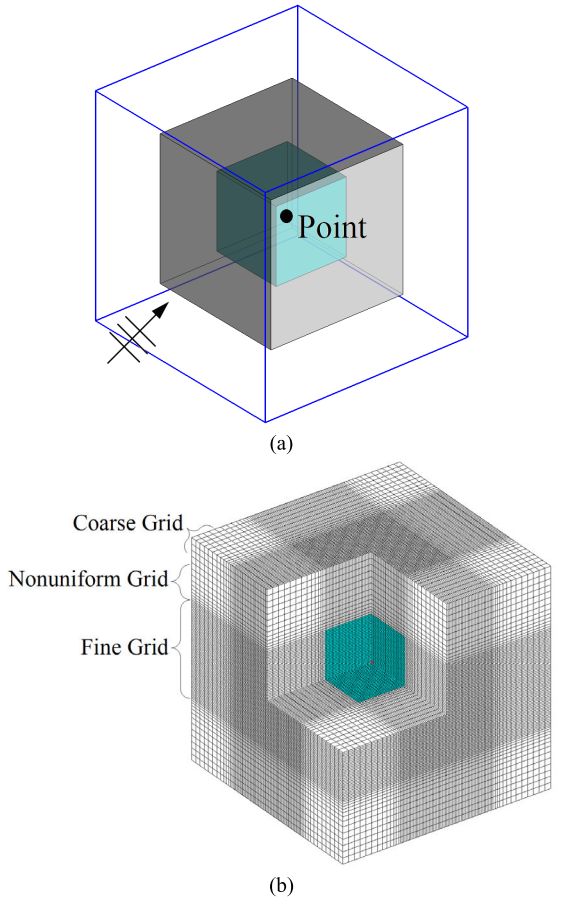

FIGURE 5. The model for the single dielectric cube: (a) the simulation model with the oblique incidence and observation point (0, 0, 0), and the gray and blue regions are respectively the air and the dielectric medium.; (b) the initialized grids for the non-uniform modeling, and the fine grids are built on the dielectric medium.

Based on the maximum frequency $f_{\max} = 1$ GHz, we can compute the spatial intervals $\Delta w_{\max} = 10$ mm in the air and $\Delta w_{\min} = 2.5$ mm in the dielectric medium, respectively. The grids numbers in three directions are respectively (161 × 161 × 161) for the fine case and (107 × 107 × 107) for the non-uniform situation. Therefore, we set $L_0 = 37.5$mm for the non-uniform regions, and then the base number L and the grid number N can be obviously captured by equations (4) and (5).

Here, we can capture the near-fields in the different frequencies at the central position of the dielectric single cubes. Shown in Fig.6, the near-fields data of E_x, E_y and E_z are adopted among the NU-FDTD with $s = 1$ and the NUSC-ADI-FDTD with $s = 1, 2, s_{\max}$ (2.53). Those results are in a good agreement even though we choose the maximum CFL factor $s_{\max}$. In addition, to further understand the accelerate effect about the NUSC-ADI-FDTD method, we record the memory and CPU time in the TABLE 3 as below.

From the TABLE 3, it can be seen that the FDTD method with non-uniform grids have the finite CFL factor $s = 1$ to limit discrete-time interval except for the SC-ADI-FDTD method. In addition, to guarantee the numerical accuracy, we

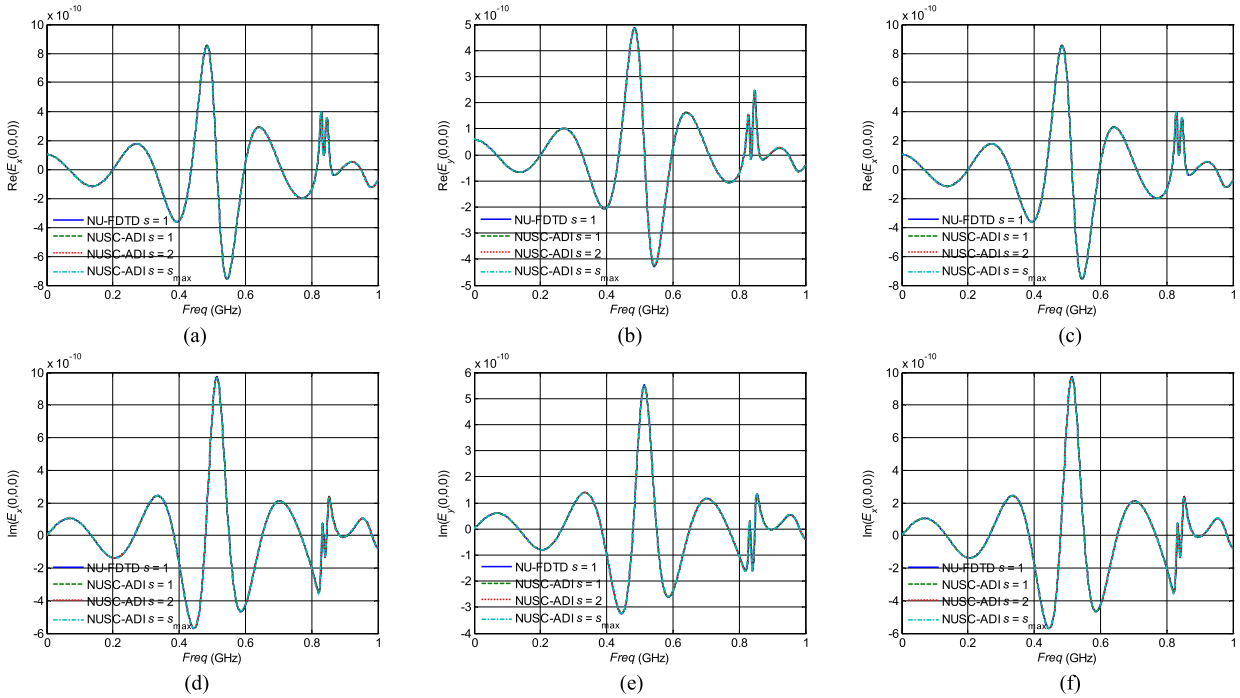

FIGURE 6. The captured frequency-domain fields at the single dielectric cube in the centre position; the real part: (a) real (E_x), (b) real (E_y), (c) real (E_z), and the imaginary part: (d) imag (E_x), (e) imag (E_y), (f) imag (E_z).

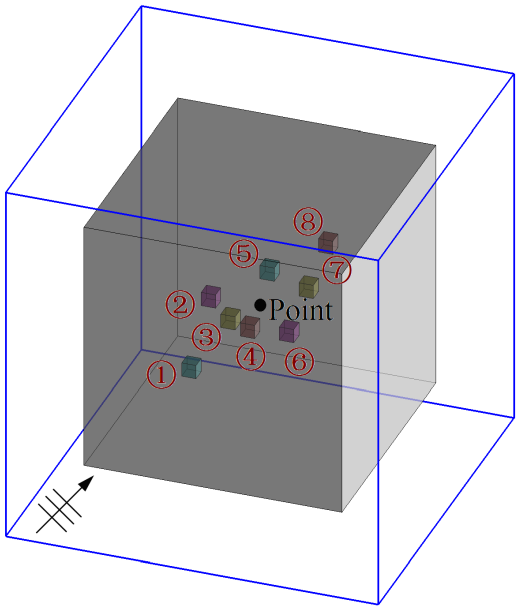

FIGURE 7. The simulation model of the local microstructure with multiple cubes.

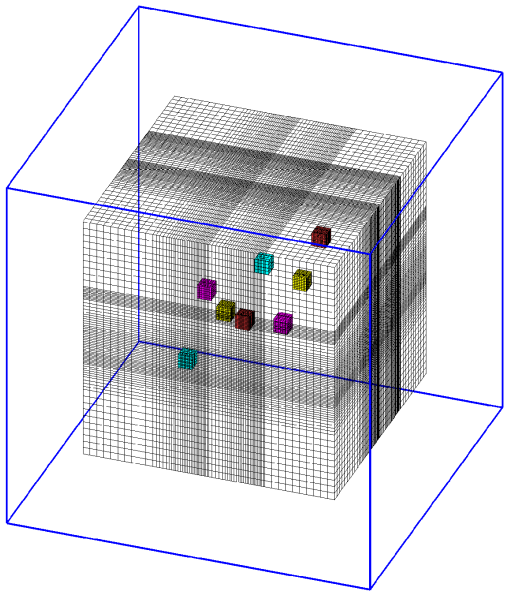

FIGURE 8. The initialized non-uniform grids of the local microstructure with multiple cubes based on the same spatial sampling densities.

TABLE 3. The computational situation among conventional NU-FDTD and NUSC-ADI-FDTD method in the single dielectric cube.

Method	CFL	Memory (MB)	CPU Time (min)
NU-FDTD	1	720.3	34.3907
NUSC-ADI-FDTD	1	1108.4	37.9892
	2	1087.3	21.4919
	$s_{max} = 2.53$	1062.8	15.6182

apply the equation (34) and obtain the maximum CFL factor for the NUSC-ADI-FDTD method for the globally-unified spatial sampling densities $Q_s = 30$ PPW. Compared with the general NU-FDTD method, the NUSC-ADI-FDTD method waste a little more memory, but it can dramatically save the CPU time.

B. LOCAL MICROSTRUCTURE WITH MULTIPLE CUBES

When facing the multiple media and the lower maximum frequency f_{max} in the electromagnetic scattering, the proposed NUSC-ADI-FDTD method has more significant advantages

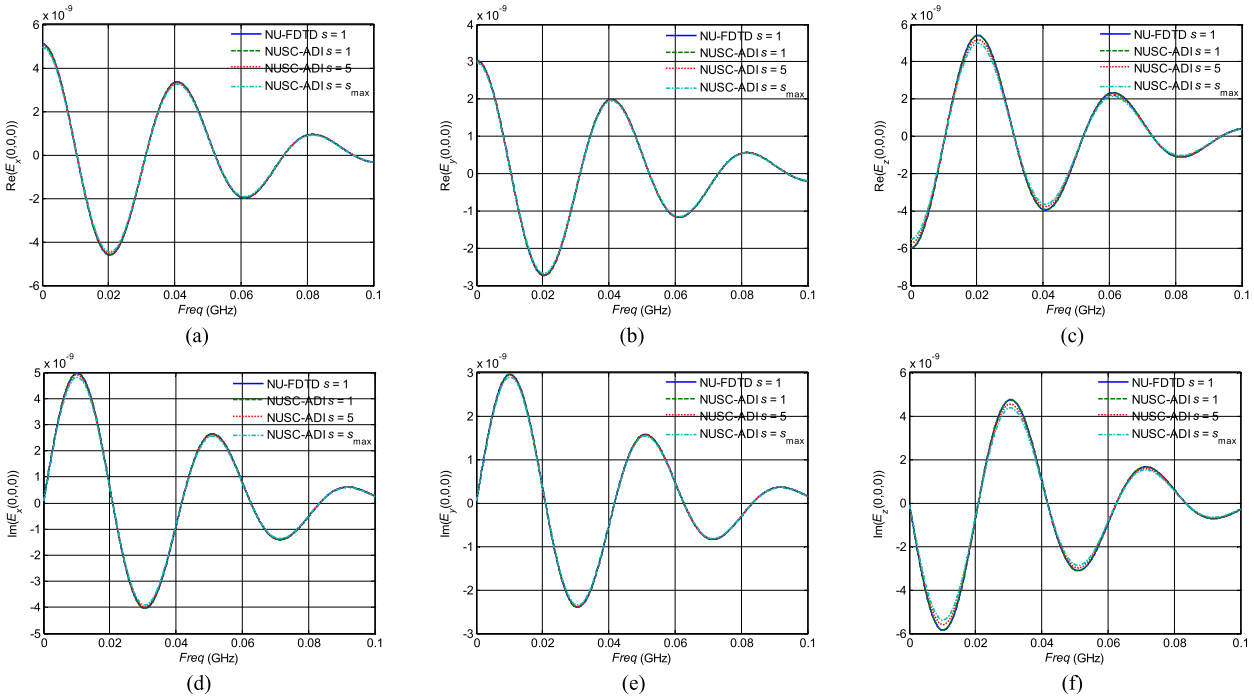

FIGURE 9. The captured frequency-domain fields at the local microstructure with multiple cubes in the centre position; the real part: (a) real (E_x), (b) real (E_y), (c) real (E_z), and the imaginary part: (d) imag (E_x), (e) imag (E_y), (f) imag (E_z).

TABLE 4. The central coordination of the eight cubes in simulation model.

No.	Coordination (mm)	No.	Coordination (mm)
①	(−70, −70,−70)	⑤	(+10, +10, +50)
②	(−50, −50,+30)	⑥	(+30, +30, −50)
③	(−30, −30, −10)	⑦	(+50, +50,+10)
④	(−10, −10, −30)	⑧	(+70, +70,+70)

TABLE 5. The computational situation among conventional NU-FDTD and NUSC-ADI-FDTD method in the local microstructure.

Method	CFL	Memory (MB)	CPU Time (min)
NU-FDTD	1	1525.5	19.6897
NUSC-ADI-FDTD	1	1913.4	24.4087
	5	1877.4	5.1060
	$s_{\max} = 8.00$	1754.1	3.2804

as the larger spatial sampling densities in the non-uniform model contribute to the greater CFL factor which can be chosen by the empirical formula. To present this superiority, we execute a local microstructure with multiple cubes shown in Fig.7 with the incident angle $\theta_{inc} = 45°$ and $\varphi_{inc} = 30°$. The eight cubes are the same geometry (20 mm × 20 mm × 20 mm) which are placed under the rectangular coordinate system shown in the TABLE 4; and those relative permittivity are respectively $\varepsilon_r = 4.0$ for No. ① and ⑤, $\varepsilon_r = 9.0$ for No. ② and ⑥, $\varepsilon_r = 16.0$ for No. ③ and ⑦, $\varepsilon_r = 25$ for No. ④ and ⑧. When considering the maximum frequency $f_{\max} = 0.10$ GHz and the spatial interval $\Delta w_{\text{air}} = 10$ mm in the air, we can obtain the globally spatial sampling densities $Q_s = 300$ PPW and ensure the maximum CFL factor $s_{\max} = 8.00$ from the equation (34). Then, the non-uniform grids for the modeling can be formed shown in Fig.8.

In the modeling initialization, the numbers of the fine and non-uniform grids are respectively (197 × 197 × 197) and (92 × 92 × 92). To further verify the high efficiency of the proposed NUSC-ADI-FDTD method, we select the CFL factors $s = 1, 5, s_{\max}$ compared with conventional NU-FDTD method. As shown in the Fig.9, it can be found that those results in the near fields maintain the reasonable accuracy. The computational situations are displayed in the TABLE 5 which introduce that the CPU Time can be obviously saved by applying the proposed NUSC-ADI-FDTD method at the CFL factor $s = s_{\max}$.

VI. CONCLUSION

In this paper, we propose the NUSC-ADI-FDTD method for solving the 3D electromagnetic scattering. By mean of the non-uniform grid initialization, we have successfully implemented the transition procedure between the coarse and fine grids. Making full application of the grids' discretization, we can execute the electromagnetic iteration of the NUSC-ADI-FDTD method. To further confirm the numerical accuracy of the NUSC-ADI-FDTD method, we can select the proper CFL factor by the empirical formula so that the efficient and accurate computation can be effectively guaranteed in the NUSC-ADI-FDTD method. Compared with the conventional FDTD in the non-uniform grids for the local micro-structure model, the computational efficiency for the NUSC-ADI-FDTD method is much higher

than the one for the NU-FDTD method due to overcoming the finite CFL limit. More importantly in the near future, the NUSC-ADI-FDTD method will pave the road for the more complex local micro-structure model in the scattering problem.

REFERENCES

[1] K. Yee, "Numerical solution of initial boundary value problems involving Maxwell's equations in isotropic media," *IEEE Trans. Antennas Propag.*, vol. 14, no. 3, pp. 302–307, May 1966.
[2] A. Taflove and S. C. Hagness, *Computational Electrodynamics: The Finite-Difference Time-Domain Method*. Boston, MA, USA: Artech House, 1998.
[3] Y. Zhang, N. Feng, H. Zheng, H. Liu, J. Zhu, and Q. H. Liu, "A corner-free truncation strategy in three-dimensional FDTD computation," *IEEE Trans. Electromagn. Compat.*, vol. 58, no. 2, pp. 512–522, Apr. 2016.
[4] Y. Zhang, N. Feng, L. Wang, Z. Guan, and Q. H. Liu, "An FDTD method for fully anisotropic periodic structures impinged by obliquely incident plane waves," *IEEE Trans. Antennas Propag.*, vol. 68, no. 1, pp. 366–376, Jan. 2020.
[5] P. Monk and E. Suli, "Error estimates for Yee's method on non-uniform grids," *IEEE Trans. Magn.*, vol. 30, no. 5, pp. 3200–3203, Sep. 1994.
[6] P. Monk and E. Suli, "A convergence analysis of Yee's scheme on non-uniform grids," *SIAM J. Numerical Anal.*, vol. 31, no. 2, pp. 393–412, 1994.
[7] E. A. Navarro, N. T. Sangary, and J. Litva, "Some considerations on the accuracy of the nonuniform FDTD method and its application to waveguide analysis when combined with the perfectly matched layer technique," *IEEE Trans. Microw. Theory Techn.*, vol. 44, no. 7, pp. 1115–1124, Jul. 1996.
[8] G. Shen, Y. Chen, and R. Mittra, "A nonuniform FDTD technique for efficient analysis of propagation characteristics of optical-fiber waveguides," *IEEE Trans. Microw. Theory Techn.*, vol. 47, no. 3, pp. 345–349, Mar. 1999.
[9] W. Yu and R. Mittra, "A technique for improving the accuracy of the nonuniform finite-difference time-domain algorithm," *IEEE Trans. Microw. Theory Techn.*, vol. 47, no. 3, pp. 353–356, Mar. 1999.
[10] W. Yu, R. Mittra, and S. Dey, "Application of the nonuniform FDTD technique to analysis of coaxial discontinuity structures," *IEEE Trans. Microw. Theory Techn.*, vol. 49, no. 1, pp. 207–209, 2001.
[11] T. Li, W. Sui, and M. Zhou, "Extending PML absorbing boundary condition to truncate microstrip line in nonuniform 3D FDTD grid," *IEEE Trans. Microw. Theory Techn.*, vol. 47, no. 9, pp. 1771–1776, Sep. 1999.
[12] Y. Zhang, B.-Q. Gao, W. Ren, Z.-H. Xue, and W.-M. Li, "Analysis and application of new quasi-network characteristics of nonuniform mesh in FDTD simulation," *IEEE Trans. Microw. Theory Techn.*, vol. 50, no. 11, pp. 2519–2526, Nov. 2002.
[13] X. Li and B. Hu, "FDTD analysis of a magneto-plasma antenna with uniform or nonuniform distribution," *IEEE Antennas Wireless Propag. Lett.*, vol. 9, pp. 175–210, 2010.
[14] A. Z. Elsherbeni and V. Demir, *The Finite-Difference Time-Domain Method For Electromagnetics with MATLAB Simulations*. Rijeka, Croatia: SciTech, 2015.
[15] L. Fezoui, S. Lanteri, S. Lohrengel, and S. Piperno, "Convergence and stability of a discontinuous Galerkin time-domain method for the 3D heterogeneous Maxwell equations on unstructured meshes," *ESAIM, Math. Model. Numer. Anal.*, vol. 39, no. 6, pp. 1149–1176, Nov. 2005.
[16] T. Namiki, "A new FDTD algorithm based on alternating-direction implicit method," *IEEE Trans. Microw. Theory Techn.*, vol. 47, no. 10, pp. 2003–2007, 1999.
[17] F. Zheng, Z. Chen, and J. Zhang, "A finite-difference time-domain method without the courant stability conditions," *IEEE Microw. Guided Wave Lett.*, vol. 9, no. 11, pp. 441–443, 1999.
[18] F. Zheng and Z. Chen, "Numerical dispersion analysis of the unconditionally stable 3-D ADI-FDTD method," *IEEE Trans. Microw. Theory Techn.*, vol. 49, no. 5, pp. 1006–1009, May 2001.
[19] J. Lee and B. Fornberg, "Some unconditionally stable time stepping methods for the 3D Maxwell's equations," *J. Comput. Appl. Math.*, vol. 166, no. 2, pp. 497–523, Apr. 2004.
[20] S.-H. Sun and C. T. M. Choi, "Envelope ADI–FDTD method and its application in three-dimensional nonuniform meshes," *IEEE Microw. Wireless Compon. Lett.*, vol. 17, no. 4, pp. 253–255, Apr. 2007.
[21] S. J. Cooke, M. Botton, T. M. Antonsen, and B. Levush, "A leapfrog formulation of the 3D ADI-FDTD algorithm," in *Proc. Workshop Comput. Electromagn. Time-Domain*, 9860035, 2007.
[22] X.-H. Wang, J.-Y. Gao, Z. Chen, and F. L. Teixeira, "Unconditionally stable one-step leapfrog ADI-FDTD for dispersive media," *IEEE Trans. Antennas Propag.*, vol. 67, no. 4, pp. 2829–2834, Apr. 2019.
[23] H. Bao and R. Chen, "An efficient domain decomposition parallel scheme for leapfrog ADI-FDTD method," *IEEE Trans. Antennas Propag.*, vol. 65, no. 3, pp. 1490–1494, Mar. 2017.
[24] K. Xu, Z. Fan, D.-Z. Ding, and R.-S. Chen, "GPU accelerated unconditionally stable crank-nicolson FDTD method for the analysis of three-dimensional microwave circuits," *Prog. Electromagn. Res.*, vol. 102, pp. 381–395, 2010.
[25] T. Hemmi, F. Costen, S. Garcia, R. Himeno, H. Yokota, and M. Mustafa, "Efficient parallel LOD-FDTD method for debye-dispersive media," *IEEE Trans. Antennas Propag.*, vol. 62, no. 3, pp. 1330–1338, Mar. 2014.
[26] D. Y. Heh and E. L. Tan, "Unconditionally stable multiple one-dimensional ADI-FDTD method for coupled transmission lines," *IEEE Trans. Antennas Propag.*, vol. 66, no. 12, pp. 7488–7492, Dec. 2018.
[27] E. Leong Tan and D. Yu Heh, "Multiple 1-D fundamental ADI-FDTD method for coupled transmission lines on mobile devices," *IEEE J. Multiscale Multiphys. Comput. Techn.*, vol. 4, pp. 198–206, Dec. 2019.
[28] H. Zheng, Y. Wu, K. Zhang, L. Wang, M. Wang, and E. Li, "Wide-band modeling on-chip spiral inductors using frequency-dependent conformal ADI-FDTD method," *IEEE Access*, vol. 7, pp. 184940–184949, 2019.
[29] J. Chen, G. Hao, and Q.-H. Liu, "Using the ADI-FDTD method to simulate graphene-based FSS at terahertz frequency," *IEEE Trans. Electromagn. Compat.*, vol. 59, no. 4, pp. 1218–1223, Aug. 2017.
[30] N. Feng, Y. Zhang, X. Tian, J. Zhu, W. T. Joines, and G. P. Wang, "System-combined ADI-FDTD method and its electromagnetic applications in microwave circuits and antennas," *IEEE Trans. Microw. Theory Techn.*, vol. 67, no. 8, pp. 3260–3270, Aug. 2019.

NAIXING FENG (Member, IEEE) received the B.S. degree in electronic science and technology and the M.S. degree in micro-electronics and solid-state electronics from Tianjin Polytechnic University, Tianjin, China, in 2010 and 2013, respectively, and the Ph.D. degree from the College of Electronic Science and Technology, Xiamen University, Xiamen, China, in 2018. From 2015 to 2016, he studied and worked as a Visiting Scholar supported by the CSC with the Department of Electrical and Computation Engineering, Duke University, USA. He is currently an Associate Professor with the College of Electronic Science and Technology, Shenzhen University, China. He has appeared around 40 papers published by refereed international journals and conference and holds one patent. His current research interests include the areas of computational electromagnetics and acoustics, photonic and nano materials, and their applications.

YUXIAN ZHANG (Member, IEEE) received the B.S. and M.S. degrees from the Tianjin University of Technology and Education, Tianjin, China, in 2012 and 2015, respectively, and the Ph.D. degree from the College of Electronic Science and Technology, Xiamen University, Xiamen, China, in 2018. He is currently an Associate Professor with the Institute of Microscale Optoelectronics, Shenzhen University, China. He has authored or coauthored 25 papers in the refereed journals and the conference proceedings and holds four Chinese patents. His current research interests include subsurface reverse-time migration imaging and computational electromagnetics, especially in the anisotropic FDTD method. He was a three-time recipient of Chinese National Scholarship and has participated in the Chinese Graduate Mathematical Contest in Modeling for five times during which he has been bestowed national awards. He has served as a reviewer for five journals.

JINFENG ZHU (Senior Member, IEEE) received the B.S. degree in electronic communication science and technology and the Ph.D. degree in physical electronics from the University of Electronic Science and Technology of China, Chengdu, Sichuan, China, in 2006 and 2012, respectively. From November 2009 to November 2011, he was a Visiting Researcher with the Device Research Laboratory, University of California, Los Angeles, CA, USA, and the Department of Electrical Engineering, University of California, under the financial support from the China Scholarship Council. Since July 2012, he has been with Xiamen University, Xiamen, Fujian, China, where he is currently an Associate Professor of electrical engineering. He has authored and coauthored more than 40 peer-reviewed journal and conference papers. His research interests include nanoantennas, nanophotonics, plasmonics, metamaterials, and van der Waals materials. He is a member of Optical Society of America, and has served as a reviewer of many academic journals, including *ACS Nano, Nanoscale, ACS Photonics, Optics Express*, and IEEE PHOTONICS JOURNAL.

QINGSHENG ZENG (Senior Member, IEEE) received the Ph.D. degree from the University of Ottawa, Canada. He has been a Research Engineer and a Senior Research Engineer with the Communications Research Centre Canada (CRC), Government of Canada. He is currently a Distinguished Professor and a Ph.D. Advisor with the Nanjing University of Aeronautics and Astronautics (NUAA), an Adjunct Professor and a Ph.D. Advisor with the University of Ottawa, Carleton University, the Université du Québec an Outaouais (UQO), and the Institut National de la Recherche Scientifique – Centre Energie, Matériauxet Télécommunications (INRS-EMT), a Guest Professor with Harbin Engineering University (HEU), Northwestern Polytechnic University (NWPU), the Beijing University of Posts and Telecommunications (BUPT), and Beijing Jiaotong University (BJTU). His work on the project Aggregate Interference Analysis and Suitability of Some Propagation Models to Ultra-Wideband Emissions in Outdoor Environments has formed one part of Consultation Paper on the Introduction of Wireless Systems Using Ultra Wideband Technology, Spectrum Management and Telecommunications Policy, Industry Canada, and has been taken as a significant contribution to International Telecommunication Union (ITU). He has published more than 130 SCI and EI indexed articles and technical reports, authored one book and coauthored two book chapters, one of which has been downloaded more than 3000 times only in one year, after it was published in 2011. He has undertaken research and teaching in several fields, including antenna analysis and design, electromagnetic compatibility and interference (EMC/EMI), ultra wideband technology, radio wave propagation, and computational electromagnetics. He is a member of the IEEE Canada Industry Relations Committee, the Strategic Projects Grant (SPG) Selection Panel (Information and Communications Technologies B) for the Natural Sciences and Engineering Research Council of Canada (NSERC), the Site Visit Committee of NSERC Industrial Research Chair (IRC), and the technical program committee member for many international and national symposia. He has won several technical and technical service awards, was ranked as one of the researchers at the Communications Research Centre Canada with the strongest impacts, in 2011, and selected as a Distinguished Expert under the Plan of Hundreds of Talents of Shanxi Province in China, in 2015, and an Overseas Prestigious Advisor of Guangdong Province, in 2017. He is the Chair of AP (Antennas and Propagation) / MTT (Microwave Theory and Techniques) Joint Chapter and the Secretary of EMC (Electromagnetic Compatibility) Chapter of IEEE Ottawa, and the technical program committee co-chair, the conference co-chair, and the session chair for many international and national symposia. He has been a reviewer of NSERC Industrial Research and Development fellowships. He also serves as the editorial board member and a reviewer for a number of technical books and scientific journals, and as a organizer, the technical program committee reviewer, a short course/workshop/tutorial presenter and a keynote speaker for many international and national symposia.

GUO PING WANG received the Ph.D. degree from Sichuan University. He is currently a Distinguished Professor with Shenzhen University, honored as the National Leading Talents in Shenzhen. He was also rewarded the National Natural Science Foundation of China for Distinguished Young Scholars, the State Council Special Allowance, and supported by the Program for New Century Excellent Talents at the University of Ministry of Education of China. His research as a Postdoctoral Fellow at Osaka University and a Visiting Scholar at the Tokyo Institute of Technology, The Hong Kong University of Science and Technology, and Nanyang Technological University. After that, he worked with Wuhan University, as the Second Rank Professor and the Distinguished Professor with Luojia Scholar. He presides more than 20 projects, including the National Science Foundation of China for Distinguished Young Scientists, the National Basic Research Program of China (973 Program), the Key Program of the National Natural Science Foundation of China, and the Program for New Century Excellent Talents in the University of Ministry of Education of China.. He has published more than 90 prereviewed journal articles with more than 50 articles being published on *Nature Communications*, *Physical Review Letters*, *Physical Review B (Rapid Communications)*, *Applied Physics Letters*, *Optics Letters*, *Optics Express*, *Nanoscale*, and *Scientific Reports*. In addition, he contributed more than 20 invited talks at international conferences and coauthored the book Plasmonic Nanoguides and Circuits. He is a Fellow of the Information Science Department and the Mathematical and Physical Science Department of the National Natural Science Foundation of China. For the excellent work, he was rewarded numerous awards, including the Second Class of the State Natural Science Award, the First Class of the Hubei Natural Science Award and the Hubei Education Achievements Award, and the First Session of the Excellent University Key Teacher Award of the Ministry of Education of China, and has obtained several innovative achievements in the research of optical metamaterials, optical super-resolution imaging and sensors, optical cloaking, nanophotonics, and other frontiers.